Applied Physics Letters

RESEARCH ARTICLE | OCTOBER 12 2020

Quadruple perovskite oxide $LaCu_3Co_2Re_2O_{12}$: A ferrimagnetic half metal with nearly 100% B-site degree of order

Zhehong Liu; Qian Sun; Xubin Ye; Xiao Wang; Long Zhou; Xudong Shen; Kai Chen; Lucie Nataf; Francois Baudelet; Stefano Agrestini; Chien-Te Chen; Hong-Ji Lin; Hari Babu Vasili; Manuel Valvidares ; Zhiwei Hu; Yi-feng Yang ; Youwen Long

Check for updates

Appl. Phys. Lett. 117, 152402 (2020)
https://doi.org/10.1063/5.0025704

View Online
Export Citation

16 April 2024 10:22:37

AIP Publishing

Applied Physics Letters ARTICLE scitation.org/journal/apl

Quadruple perovskite oxide $LaCu_3Co_2Re_2O_{12}$: A ferrimagnetic half metal with nearly 100% B-site degree of order

Cite as: Appl. Phys. Lett. **117**, 152402 (2020); doi: 10.1063/5.0025704
Submitted: 18 August 2020 · Accepted: 21 September 2020 ·
Published Online: 12 October 2020

View Online Export Citation CrossMark

Zhehong Liu,[1,2] Qian Sun,[1] Xubin Ye,[1,2] Xiao Wang,[3] Long Zhou,[1,2] Xudong Shen,[1,2] Kai Chen,[4] Lucie Nataf,[5] Francois Baudelet,[5] Stefano Agrestini,[6] Chien-Te Chen,[7] Hong-Ji Lin,[7] Hari Babu Vasili,[6] Manuel Valvidares,[6] Zhiwei Hu,[3] Yi-feng Yang,[1,2,8,a)] and Youwen Long[1,2,8,a)]

AFFILIATIONS

[1]Beijing National Laboratory for Condensed Matter Physics, Institute of Physics, Chinese Academy of Sciences, Beijing 100190, China
[2]School of Physical Sciences, University of Chinese Academy of Sciences, Beijing 100049, China
[3]Max Planck Institute for Chemical Physics of Solids, Nöthnitzer Straße 40, 01187 Dresden, Germany
[4]Helmholtz-Zentrum Berlin fur Materialien und Energie, Albert-Einstein-Str..15, 12489 Berlin, Germany
[5]Synchrotron SOLEIL, L'Orme des Merisiers, Saint-Aubin, 91192 Gif-sur-Yvette Cedex, France
[6]ALBA Synchrotron Light Source, Cerdanyola del Valles, 08290 Barcelona, Spain
[7]National Synchrotron Radiation Research Center, Hsinchu 30076, Taiwan
[8]Songshan Lake Materials Laboratory, Dongguan, Guangdong 523808, China

[a)]**Authors to whom correspondence should be addressed:** yifeng@iphy.ac.cn and ywlong@iphy.ac.cn

ABSTRACT

An *A*- and *B*-site ordered quadruple perovskite oxide $LaCu_3Co_2Re_2O_{12}$ was synthesized at 9 GPa and 1323 K. The compound possesses a *Pn*-3 space group, where both *A* and *B* sites are orderly occupied by different cations with a nearly 100% degree of order. Bond valence sum calculations and x-ray absorption spectroscopy confirm the charge distribution to be $LaCu^{2+}{}_3Co^{2+}{}_2Re^{5.5+}{}_2O_{12}$. A ferrimagnetic phase transition is found to occur around 150 K due to the $Cu^{2+}(\uparrow)$-$Co^{2+}(\uparrow)$-$Re^{5.5+}(\downarrow)$ spin coupling found by x-ray magnetic circular dichroism at Cu-, Co-, and Re-$L_{2,3}$ edges. The magnetoresistance effects as well as the first-principle calculations indicate the half-metallic nature for $LaCu_3Co_2Re_2O_{12}$ with a wider energy gap at the up-spin channel and a conducting band at the down-spin channel.

Published under license by AIP Publishing. https://doi.org/10.1063/5.0025704

Half metals have been attracting great interest due to their potential technological applications in high-efficiency magnetic sensors, computer memories, and magnetic recording.[1–6] The electrical transport of an ideal half metal is featured by 100% spin polarization, i.e., one spin channel accounts for metallic conductivity, while the other displays insulating behavior.[1–4] To date, different kinds of half metals such as Heusler alloy NiMnSb,[6] rutile CrO_2,[7,8] spinel Fe_3O_4,[9,10] hole-doped Mott insulator $La_{1-x}Sr_xMnO_3$,[11–13] pyrochlore $Tl_2Mn_2O_7$,[14] double perovskite Sr_2FeMoO_6,[15] and zinc blende CrTe/Se[16] have already been discovered. Among them, the *B*-site ordered double perovskite Sr_2FeMoO_6 is one of the most interesting examples due to the high ferrimagnetic (FiM) ordering temperature $T_C \approx 410$ K, which arises from the antiferromagnetically coupled Fe^{3+}-Mo^{5+} interaction.[15] For a *B*-site ordered double perovskite $A_2BB'O_6$, when three quarters of the *A* site are replaced by a transition metal *A*′, both *A*- and *B*-site ordered quadruple perovskite with a chemical formula $AA'_3B_2B'_2O_{12}$ is possible to form. In such a peculiar two-site ordered perovskite system, the Cu^{2+} and Mn^{3+} ions with strong Jahn-Teller distortion often occupy the *A*′ site due to the square-planar coordination, as exemplified by $CaCu_3Fe_2Re_2O_{12}$,[17] $Ca/NaCu_3Fe_2Os_2O_{12}$,[18,19] and $LaMn_3Ni_2Mn_2O_{12}$.[20] In particular, $CaCu_3Fe_2Re_2O_{12}$ and $NaCu_3Fe_2Os_2O_{12}$ exhibit half-metallic properties with FiM spin ordering well above room temperature.[17,18] However, in these systems, the low-field magnetoresistance (MR) is very small, which is detrimental for potential applications. Since the MR effects of ordered perovskites are intimately related to the antisite disorder between the *B*- and *B*′-site ions, it is, therefore, desirable to improve the degree of order toward a nearly 100% value.[17,18] In addition, a wider half-metallic

16 April 2024 10:22:37

energy gap is favorable to suppress the spin-flip transition caused by thermal excitation of carriers so that the half-metallic performance can be preserved in the working temperature range. In this article, we report the synthesis of both *A*- and *B*-site ordered quadruple perovskite oxide $LaCu_3Co_2Re_2O_{12}$ (LCCRO), in which Co and Re are orderly distributed at the *B*/*B*′ sites with an almost 100% degree of order. As a result, the compound displays an enhanced low-field MR effect. Moreover, a wide up-spin energy gap is found to occur by theoretical calculations.

The experimental details are described in the supplementary material. Figure 1(a) shows the x-ray diffraction (XRD) pattern of LCCRO measured at room temperature together with the Rietveld refinement results. All the diffraction peaks can be indexed based on a cubic structure framework. The Rietveld analysis reveals that LCCRO crystallizes to an $AA'_3B_2B'_2O_{12}$-type quadruple perovskite structure with space group *Pn*-3, where La and Cu are 1:3 ordered at *A* and *A*′ sites, while Co and Re are also orderly distributed at *B* and *B*′ sites with a 1:1 ratio, respectively (see Table SI for detailed atomic positions). As shown in Fig. 1(a), one can find a series of sharp diffraction peaks with the Miller indices $h+k+l$ = odd, such as (111), (311), and (331) peaks, indicating the formation of order for the *B*-site Co and *B*′-site Re at a rock salt-type fashion. Since the x-ray scattering factors of Co and Re are different considerably, one can examine the antisite effect between these two atoms by refining the occupancy parameter. During the refinement, we find that the occupancy factor for both Co and Re is almost 100%, revealing the negligible Co–Re antisite disorder. Actually, if a small amount of antisite occupancy like 5% is constrained for Co or Re, the Co–O or Re–O bond length becomes unreasonable. Therefore, the occupancy factors of Co and Re are fixed to be unity to refine other structural parameters, and a satisfied goodness-of-fit is obtained (e.g., R_{wp} = 3.34%, R_p = 2.1%). The high *B*/*B*′-site ordering in the current LCCRO differs from that observed in the isostructural compounds $CaCu_3Fe_2Re_2O_{12}$ (93.8%) and $CaCu_3Fe_2Os_2O_{12}$ (88.2%). Figure 1(b) shows the schematic crystal structure of LCCRO. As observed in a simple ABO_3 perovskite, the *B*/*B*′-site Co/Re forms six-oxygen-coordination octahedra, whereas the *A*′-site Cu forms four-oxygen-coordination squares. According to the refined bond lengths listed in Table SI, the bond valence sum (BVS) calculations illustrate that the valence states of Cu and Co are very close to +2. The Re–O bond length observed in LCCRO (1.917 Å) is shorter than that in $CaCu_3Fe_2Re^{5+}{}_2O_{12}$ (1.934 Å)[17] but longer than that in $Sr_2MgRe^{6+}O_6$ (1.912 Å in average),[21] suggesting an intermediate Re valence state between Re^{5+} and Re^{6+}, in agreement with x-ray absorption spectroscopy (XAS) shown below.

The soft x-ray XAS spectra at the 3*d* element $L_{2,3}$ edges are highly sensitive to the valence state and local environment. Figure 2(a) shows the Cu-$L_{2,3}$ XAS of LCCRO together with that of the quadruple perovskite $CaCu_3Ti_4O_{12}$ as a Cu^{2+} reference. One can see that the Cu-$L_{2,3}$ edges of LCCRO have a similar single symmetry peak and energy position with those of $CaCu_3Ti_4O_{12}$ and also CuO as Ref. 22 shows, indicating the presence of Cu^{2+}. As shown in Fig. 2(b), CoO and $EuCoO_3$[23] are used as high-spin Co^{2+} and low-spin Co^{3+} references with CoO_6 octahedral coordination, respectively. The Co-$L_{2,3}$ spectrum of LCCRO shifts to lower energy relative to Co^{3+} reference $EuCoO_3$ by more than 1 eV but locates at a similar energy to that of CoO,

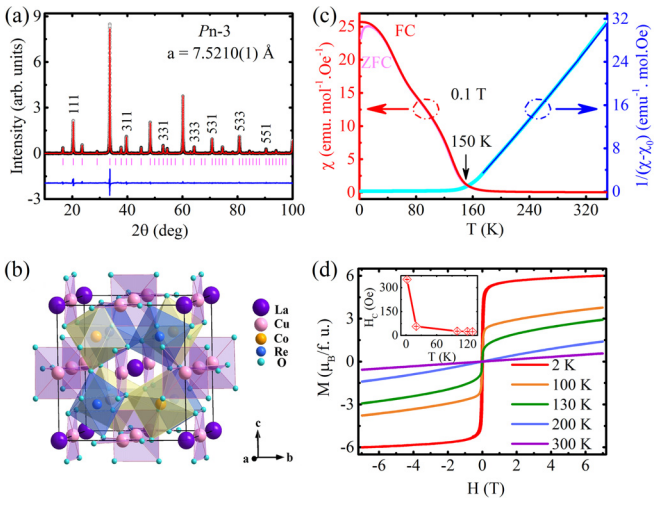

FIG. 1. (a) XRD pattern of LCCRO together with the Rietveld refinement results based on space group *Pn*-3. The observed (black circles), calculated (red line), and difference (bottom blue line) profiles are shown. The ticks indicate the allowed Bragg reflections. (b) Schematic crystal structure of LCCRO. (c) Temperature dependence of magnetic susceptibility and the inverse susceptibility. The blue line shows the Curie–Weiss fitting above 175 K. (d) Field dependence of magnetization measured at some selected temperatures. The inset shows the values of coercive field H_C below T_C.

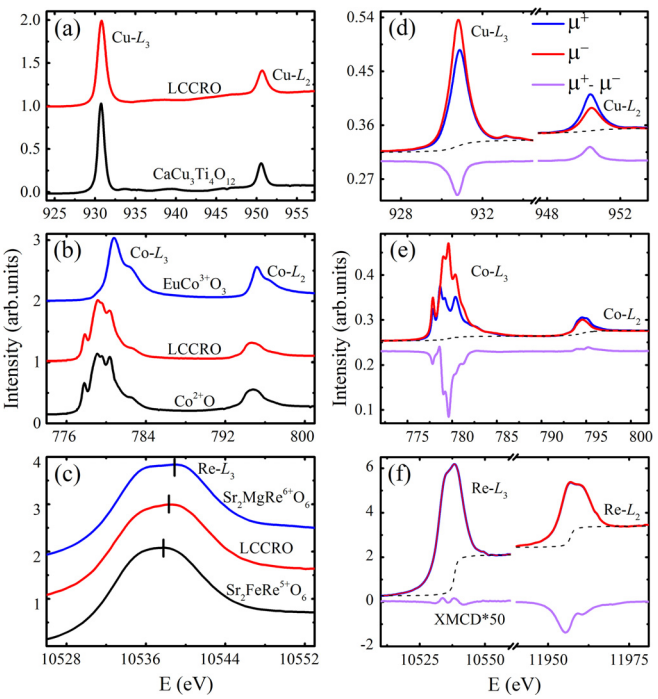

FIG. 2. XAS of (a) Cu-$L_{2,3}$ edges, (b) Co-$L_{2,3}$ edges, and (c) Re-L_3 edges for LCCRO. Some references are also shown for comparison. XMCD for (d) Cu- and (e) Co-$L_{2,3}$ edges measured at 10 K and 6 T and (f) Re-$L_{2,3}$ edges measured at 10 K and 1.3 T. The photon spin is aligned parallel (μ^+ blue line) and antiparallel (μ^- red line) to the applied magnetic field, respectively. The difference spectra (μ^+-μ^-) are shown in purple lines.

16 April 2024 10:22:37

Published under license by AIP Publishing

suggesting the formation of the Co^{2+} state in LCCRO. The comparable multiplet spectral features between LCCRO and CoO indicate Co^{2+} to be a high-spin state with $S = 3/2$.[24] Figure 2(c) shows the XAS at the Re-L_3 edge of LCCRO together with $Sr_2FeRe^{5+}O_6$[25] and $Sr_2MgRe^{6+}O_6$ as the Re^{5+} and Re^{6+} references, respectively. Obviously, the energy position of LCCRO locates at the middle between these two references, indicating an average $Re^{5.5+}$ state in LCCRO fulfilling the charge balance requirement. Therefore, the XAS data confirm that the charge combination of LCCRO is $LaCu^{2+}{}_3Co^{2+}{}_2Re^{5.5+}{}_2O_{12}$, consistent with the BVS analysis. The average $Re^{5.5+}$ charge state would correspond to a mixture of Re^{5+} and Re^{6+} with a 1:1 mole ratio. The considerable charge and ionic radius differences between Co^{2+} and $Re^{5.5+}$ favor the formation of high *B*-site degree of order.[26]

Figure 1(c) shows the temperature dependence of magnetic susceptibility for LCCRO measured at 0.1 T using both zero-field-cooling (ZFC) and field-cooling (FC) modes. With decreasing temperature to $T_C \approx 150$ K, the susceptibility experiences a sharp increase, suggesting the occurrence of a ferromagnetic (FM) or FiM phase transition. Above 175 K, the inverse magnetic susceptibility (χ-χ_0) can be reproduced by the modified Curie–Weiss (CW) law with the expression $(\chi\text{-}\chi_0)^{-1} = (T-\theta)/C$, where χ_0 is a temperature independent term containing the Van Vleck paramagnetism and core diamagnetism. A small value of $\chi_0 = -2.45 \times 10^{-3}$ emu·mol^{-1}·Oe^{-1} is obtained from the fitting. The fitted Weiss temperature is $\theta = 151$ K, in coherence with the FM/FiM ordering occurring at $T_C \approx 150$ K. According to the Curie constant (C = 6.86 emu·K·mol^{-1}·Oe^{-1}), the effective magnetic moment is calculated to be $\mu_{eff} \approx 7.41\ \mu_B$/f.u. If one considers the spin moments of the three transition-metal ions (Cu^{2+}, Co^{2+}, and $Re^{5.5+}$) as well as the orbital moment of the $Re^{5.5+}$ ion, the effective moment of LCCRO in theory should be 6.62 μ_B/f.u., which is somewhat less than the fitting result due to the presence of orbital moment of Co^{2+} as will be shown later.

The field-dependent magnetization provides further evidence for the FM/FiM ordering of LCCRO. As shown in Fig. 1(d), the linear magnetization is observed above T_C (e.g., at 200 and 300 K), as expected from the paramagnetism. Below T_C, however, magnetic hysteresis behavior is found to occur, confirming the FM/FiM ordering. For example, at 2 K, the magnetization increases sharply with the field up to about 0.2 T, and the saturated magnetic moment observed at 7 T is 6.0 μ_B/f.u. In addition, the coercive force of LCCRO is quite small and slightly increases on cooling. Specifically, it increases from 20 Oe at 130 K to 350 Oe at 2 K. Since Cu^{2+}, Co^{2+}, and $Re^{5.5+}$ are all possible to contribute to the magnetic ordering in LCCRO, there exist four different collinear spin coupling between them, i.e., the FM $Cu^{2+}(\uparrow)$-$Co^{2+}(\uparrow)$-$Re^{5.5+}(\uparrow)$, and the FiM $Cu^{2+}(\downarrow)$-$Co^{2+}(\uparrow)$-$Re^{5.5+}(\uparrow)$, $Cu^{2+}(\uparrow)$-$Co^{2+}(\downarrow)$-$Re^{5.5+}(\uparrow)$, and $Cu^{2+}(\uparrow)$-$Co^{2+}(\uparrow)$-$Re^{5.5+}(\downarrow)$. If we only consider the contribution of spin moment in a localized electronic assumption, the saturated magnetic moment generated by these spin modes is 12, 6, 0, and 6 μ_B/f.u., respectively. By comparison with experiment, the FiM $Cu^{2+}(\downarrow)$-$Co^{2+}(\uparrow)$-$Re^{5.5+}(\uparrow)$ and $Cu^{2+}(\uparrow)$-$Co^{2+}(\uparrow)$-$Re^{5.5+}(\downarrow)$ interactions are most probably to occur.

To confirm the detailed FiM spin coupling, we utilized the x-ray magnetic circular dichroism spectroscopy (XMCD) at the $L_{2,3}$ edges of Cu, Co, and Re. As shown in Figs. 2(d)–2(f), the same negative (positive) XMCD signs are observed at the L_3 (L_2) edges for Cu and Co. In contrast, the XMCD signs of Re at L_3 and L_2 edges are opposite to those of Cu and Co, providing convincing evidence for the occurrence of $Cu^{2+}(\uparrow)$-$Co^{2+}(\uparrow)$-$Re^{5.5+}(\downarrow)$ FiM coupling in LCCRO. Actually, such a kind of FiM coupling is also observed in other isostructural compounds such as $CaCu_3Fe_2Re_2O_{12}$ and $Ca/NaCu_3Fe_2Os_2O_{12}$.[17–19] Another advantage of XMCD is that it is a unique spectroscopic tool to determine the spin magnetic moment (M_{spin}) and orbital moment (M_{orb}) separately for each element by using the sum rules as follows:[27,28]

$$M_{orb} = Lz = -\frac{4\int_{L_3+L_2}(\mu^+ - \mu^-)d\omega}{3\int_{L_3+L_2}(\mu^+ + \mu^-)d\omega}(10 - N_d), \quad (1)$$

$$M_{spin} = 2Sz + 7(Tz) = -\frac{2\int_{L_3}(\mu^+ - \mu^-)d\omega - 4\int_{L_2}(\mu^+ - \mu^-)d\omega}{\int_{L_3+L_2}(\mu^+ + \mu^-)d\omega}(10 - N_d). \quad (2)$$

Here, N_d is the electron occupation number and $\langle Tz \rangle$ is the intra-atomic magnetic-dipole moment, which is negligible compared to M_{spin} in an octahedral (O_h) symmetry coordination.[28] The calculated results are shown in Table SII. The total magnetic moment was estimated to be 5.8 μ_B, which is comparable to the value of 6.0 μ_B measured at 2 K and 7 T in magnetization. Note that the M_{orb} of Co^{2+} contributes about 0.73 μ_B, which cannot be neglected as other 3*d* transition-metal ions caused by the crystal field. Similar results are also observed in some high-spin Co^{2+} compounds like Ca_3CoRhO_6,[23] CoV_2O_6,[29] and La_2MnCoO_6.[30]

Figure 3(a) shows the temperature dependence of resistivity for LCCRO. At 300 K, the resistivity value is only about 0.14 Ω cm^{-1}. With decreasing temperature, the resistivity slightly increases to about 0.50 Ω cm^{-1} at 2 K without visible anomaly occurring near T_C. On the

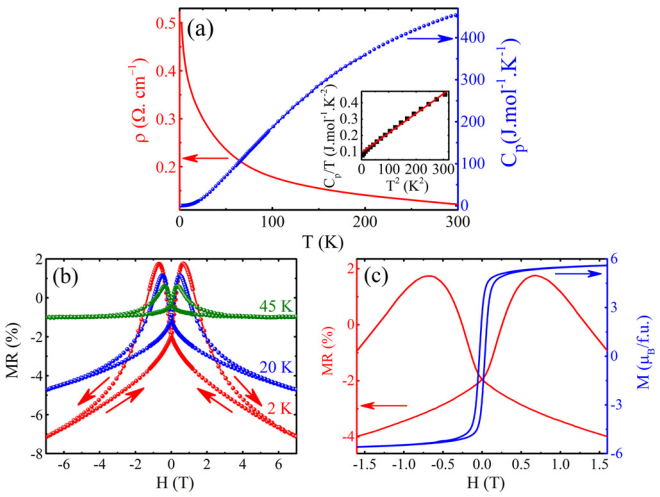

FIG. 3. (a) Temperature dependence of resistivity and specific heat at zero field. The inset shows the fitting of specific heat below 18 K using the function $C_p/T = \gamma + \beta T^2$, which yields $\gamma = 95.4(4)$ mJ/mol K^2 and $\beta = 1.2(2)$ mJ/mol K^4. (b) Field-dependent MR effects measured at selected temperatures. (c) Comparison of low-field MR and magnetization behavior at 2 K.

16 April 2024 10:22:37

Published under license by AIP Publishing

other hand, if one fits the low-temperature specific heat [see the inset of Fig. 3(a)], a considerable electron contribution is found, as reflected by the fitted Sommerfeld coefficient $\gamma = 95.4(4)$ mJ/mol K^2, suggesting an itinerant electronic behavior of LCCRO. Therefore, the small upturn of resistivity on cooling most probably arises from the grain boundary effects due to the polycrystalline nature. Note that there is no clear anomaly in the specific heat around T_C, probably due to the formation of some short-range spin correlations, which release most of the magnetic entropy change above Tc. The field-dependent MR depicted in Fig. 3(b) shows a butterfly like MR feature, indicating spin-dependent tunneling behavior originating from spin-polarized conduction electrons through grain boundaries.[31] When the magnetic hysteresis curves for the low-field MR and magnetization are compared at 2 K as shown in Fig. 3(c), it is observed that the hysteresis field of MR (6700 Oe) is much larger than that of magnetization (350 Oe). This behavior is similar to that observed in other half-metallic perovskite oxides such as Sr_2FeMoO_6,[15] $CaCu_3Fe_2Re_2O_{12}$,[17] and $NaCu_3Fe_2Os_2O_{12}$,[18] indicating a spin-valve-type MR contributed by the intergrain tunnelling of spin-polarized conduction carriers.[32] However, the current LCCRO with a nearly 100% B-site degree of order exhibits an enhanced low-field MR value (~3.5% at 2 K and 1 T) compared with the isostructural compounds with some antisite occupations like $CaCu_3Fe_2Re_2O_{12}$[17] (~1.5% at 10 K and 1 T) and $NaCu_3Fe_2Os_2O_{12}$[18] (~0.1% at 2 K and 1 T). This result suggests that the increase in the B-site degree of order favors the MR behavior and, therefore, the half-metallic performance.

To further confirm the magnetic ground state as well as the electronic properties of LCCRO, spin-polarized density functional theory (DFT) calculations, based on the generalized-gradient approximation (GGA), taking into account both the electronic correlation effect (U) and spin–orbit coupling (SOC), have been carried out for four different magnetic configurations, i.e., $Cu^{2+}(\uparrow)$-$Co^{2+}(\uparrow)$-$Re^{5.5+}(\downarrow)$, $Cu^{2+}(\uparrow)$-$Co^{2+}(\downarrow)$-$Re^{5.5+}(\downarrow)$, $Cu^{2+}(\uparrow)$-$Co^{2+}(\downarrow)$-$Re^{5.5+}(\uparrow)$, and $Cu^{2+}(\uparrow)$-$Co^{2+}(\uparrow)$-$Re^{5.5+}(\uparrow)$. Detailed parameters can be found in the supplementary material. The final results of GGA, GGA+U, and GGA+U+SOC calculations all converge to the observed $Cu^{2+}(\uparrow)$-$Co^{2+}(\uparrow)$-$Re^{5.5+}(\downarrow)$ FiM ground state with a total magnetic moment about 6.0 μ_B/f.u. Figure 4 presents the spin-resolved density of states (DOS) and band structures from GGA+U, with a typical choice of the Coulomb interaction of 5 eV for Cu, 4 eV for Co, and 2 eV for Re. The calculated magnetic moments inside the muffin-tin spheres for Cu, Co, and Re are 0.51, 2.64, and −0.69 μ_B, respectively, which are smaller than the ideal 2S values due to hybridization with O 2p orbitals and are found to be only slightly changed by SOC. The calculations also suggest that LCCRO is a half metal with fully spin-polarized conduction electrons. We see a large bandgap (about 1.9 eV) in the up(majority)-spin band and only down(minority)-spin bands of mainly Co 3d and Re 5d (hybridized with O 2p states) cross the Fermi level. The magnitude of the gap is reduced to about 0.5 eV in GGA, but the qualitative features, namely, the magnetic configuration of the ground state and its half-metallic property, are unchanged in all of our calculations.

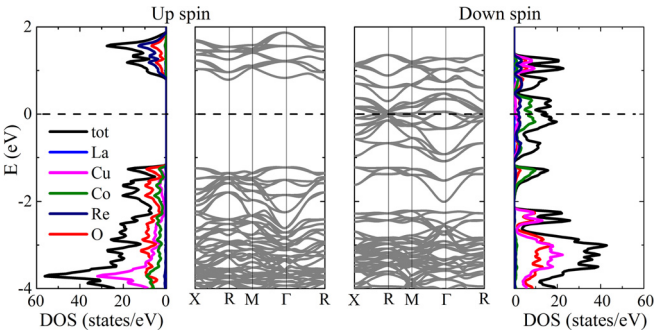

FIG. 4. Density of states and band structures for up-spin and down-spin electrons calculated by GGA+U. Total DOS (black curves) and partial DOS of Cu (pink curves), Co (green curves), Re (navy curves), and O (red curves) are shown.

In summary, an A- and B- site ordered quadruple perovskite oxide $LaCu_3Co_2Re_2O_{12}$ was prepared at 9 GPa and 1323 K with space group Pn-3. The charge distribution was determined to be $LaCu^{2+}{}_3Co^{2+}{}_2Re^{5.5+}{}_2O_{12}$ by BVS and XAS methods. The compound experiences a FiM phase transition around 150 K. Magnetization and XMCD results indicate a $Cu^{2+}(\uparrow)$-$Co^{2+}(\uparrow)$-$Re^{5.5+}(\downarrow)$ FiM coupling, in agreement with DFT calculations. Electrical transport measurements suggest a spin-valve-type half metallic behavior with an enhanced low-field MR effect. Theoretical calculations further support the conclusion that the FiM ground state is half-metallic with minority-spin bands crossing the Fermi level and a large majority-spin bandgap being opened. The present work provides a rare B-site nearly 100% ordered perovskite system with enhanced half-metallic performance.

See the supplementary material for experimental details, the relevant structure parameters and valence states (Table SI), and the orbital and spin moments of Cu^{2+}, Co^{2+}, and $Re^{5.5+}$ ions (Table SII).

This work was supported by the National Key R&D Program of China (Grant Nos. 2018YFA0305700 and 2018YFE0103200), the National Natural Science Foundation of China (Grant Nos. 11934017, 51772324, 11921004, 11904392, and 11974397), and the Chinese Academy of Sciences (Grant Nos. XDB33000000 and QYZDB-SSW-SLH013). We acknowledge the support from the Max Planck-POSTECH-Hsinchu Center for Complex Phase Materials. The research in Dresden was partially supported by the Deutsche Forschungsgemeinschaft through No. SFB 1143. We acknowledge beamtime at ALBA BL29 BOREAS via Proposal ID No. 2018082933.54.

DATA AVAILABILITY

The data that support the findings of this study are available in the supplementary material and from the corresponding author upon reasonable request.

REFERENCES

[1]R. J. Celotta and D. T. Pierce, Science **234**, 333–340 (1986).
[2]I. Žutic, J. Fabian, and S. D. Sarma, Rev. Mod. Phys. **76**, 323 (2004).
[3]M. I. Katsnelson, V. Y. Irkhin, L. Chioncel, A. I. Lichtenstein, and R. A. de Groot, Rev. Mod. Phys. **80**, 315–378 (2008).
[4]A. Fert, Rev. Mod. Phys. **80**, 1517–1530 (2008).
[5]X.-L. Wang, S. X. Dou, and C. Zhang, NPG Asia Mater. **2**, 31–38 (2010).
[6]R. A. de Groot, F. M. Mueller, P. G. van Engen, and K. H. J. Buschow, Phys. Rev. Lett. **50**, 2024–2027 (1983).
[7]K.-H. Schwarz, J. Phys. F **16**, L211–L215 (1986).

16 April 2024 10:22:37

Published under license by AIP Publishing

[8]R. Wiesendanger, H.-J. Güntherodt, G. Güntherodt, R. J. Gambino, and R. Ruf, Phys. Rev. Lett. **65**, 247–250 (1990).
[9]A. Yanase and K. Siratori, J. Phys. Soc. Jpn. **53**, 312–317 (1984).
[10]I. V. Shvets, R. Wiesendanger, D. Biirgler, G. Tarrach, H.-J. GCintherodt, and J. M. D. Coey, J. Appl. Phys. **71**, 5489–5499 (1992).
[11]Y. Tokura, A. Urushibara, Y. Moritomo, T. Arima, A. Asamitsu, G. Kido, and N. Furukawa, J. Phys. Soc. Jpn. **63**, 3931–3935 (1994).
[12]S. Jin, T. H. Tiefel, M. McCormack, R. A. Fastnacht, R. Ramesh, and L. H. Chen, Science **264**, 413–415 (1994).
[13]A. P. Ramirez, J. Phys.: Condens. Matter **9**, 8171–8199 (1997).
[14]Y. Shimakawa, Y. Kubo, and T. Manako, Nature **379**, 53–55 (1996).
[15]K.-I. Kobayashi, T. Kimura, H. Sawada, K. Terakura, and Y. Tokura, Nature **395**, 677–680 (1998).
[16]W.-H. Xie, Y.-Q. Xu, and B.-G. Liu, Phys. Rev. Lett. **91**, 037204 (2003).
[17]W. T. Chen, M. Mizumaki, H. Seki, M. S. Senn, T. Saito, D. Kan, J. P. Attfield, and Y. Shimakawa, Nat. Commun. **5**, 3909 (2014).
[18]X. Wang, M. Liu, X. Shen, Z. Liu, Z. Hu, K. Chen, P. Ohresser, L. Nataf, F. Baudelet, H. J. Lin, C. T. Chen, Y. L. Soo, Y. Yang, C. Jin, and Y. Long, Inorg. Chem. **58**, 320 (2019).
[19]H. Deng, M. Liu, J. Dai, Z. Hu, C. Kuo, Y. Yin, J. Yang, X. Wang, Q. Zhao, Y. Xu, Z. Fu, J. Cai, H. Guo, K. Jin, T. Pi, Y. Soo, G. Zhou, J. Cheng, K. Chen, P. Ohresser, Y. Yang, C. Jin, L. H. Tjeng, and Y. Long, Phys. Rev. B **94**, 024414 (2016).
[20]Y.-Y. Yin, M. Liu, J.-H. Dai, X. Wang, L. Zhou, H. Cao, C. Cruz, C.-T. Chen, Y. Xu, X. Shen, R. Yu, J. A. Alonso, A. Munoz, Y.-F. Yang, C. Jin, Z. Hu, and Y. Long, Chem. Mater. **28**, 8988–8996 (2016).
[21]C. R. Wiebe, J. E. Greedan, P. P. Kyriakou, G. M. Luke, J. S. Gardner, A. Fukaya, I. M. Gat-Malureanu, P. L. Russo, A. T. Savici, and Y. J. Uemura, Phys. Rev. B **68**, 134410 (2003).
[22]L. H. Tjeng, C. T. Chen, and S.-W. Cheong, Phys. Rev. B **45**, 8205 (1992).
[23]Z. Hu, H. Wu, M. W. Haverkort, H. H. Hsieh, H.-J. Lin, T. Lorenz, J. Baier, A. Reichl, I. Bonn, C. Felser, A. Tanaka, C. T. Chen, and L. H. Tjeng, Phys. Rev. Lett. **92**(20), 207402 (2004).
[24]T. Burnus, Z. Hu, H. Wu, J. C. Cezar, S. Niitaka, H. Takagi, C. F. Chang, N. B. Brookes, H.-J. Lin, L. Y. Jang, A. Tanaka, K. S. Liang, C. T. Chen, and L. H. Tjeng, Phys. Rev. B **77**, 205111 (2008).
[25]J. Herrero-Martin, G. Subias, J. Blasco, J. Garcia, and M. C. Sanchez, J. Phys.: Condens. Matter **17**, 4963–4976 (2005).
[26]S. Vasala and M. Karppinen, Prog. Solid State Chem. **43**, 1–36 (2015).
[27]B. T. Thole, P. Carra, F. Sette, and G. van der Laan, Phys. Rev. Lett. **68**, 1943 (1992).
[28]P. Carra, B. T. Thole, M. Altarelli, and X. Wang, Phys. Rev. Lett. **70**, 694 (1993).
[29]N. Hollmann, S. Agrestini, Z. Hu, Z. He, M. Schmidt, C.-Y. Kuo, M. Rotter, A. A. Nugroho, V. Sessi, A. Tanaka, N. B. Brookes, and L. H. Tjeng, Phys. Rev. B **89**, 201101(R) (2014).
[30]T. Burnus, Z. Hu, H. H. Hsieh, V. L. J. Joly, P. A. Joy, M. W. Haverkort, H. Wu, A. Tanaka, H.-J. Lin, C. T. Chen, and L. H. Tjeng, Phys. Rev. B **77**, 125124 (2008).
[31]H. Y. Hwang, S. W. Cheong, N. P. Ong, and B. Batlogg, Phys. Rev. Lett. **77**, 2041–2044 (1996).
[32]D. D. Sarma, S. Ray, K. Tanaka, M. Kobayashi, A. Fujimori, P. Sanyal, H. R. Krishnamurthy, and C. Dasgupta, Phys. Rev. Lett. **98**, 157205 (2007).

16 April 2024 10:22:37

Published under license by AIP Publishing